


OCTOBER 01 2024

Flyback sonic booms from Falcon-9 rockets: Measured data and some considerations for future models **FREE**

Mark C. Anderson; Kent L. Gee ; Kaylee Nyborg



Proc. Mtgs. Acoust. 54, 040005 (2024)

<https://doi.org/10.1121/2.0001916>



Articles You May Be Interested In

Overview and spectral analysis of the Falcon-9 SARah-1 launch and reentry sonic boom

Proc. Mtgs. Acoust. (October 2023)

Analysis of sonic booms from Falcon 9 booster landings

J Acoust Soc Am (April 2022)

Acoustic energy harvesting using an electromechanical Helmholtz resonator

J. Acoust. Soc. Am. (April 2008)



ASA

Advance your science and career as a member of the
Acoustical Society of America

[LEARN MORE](#)



Acoustics Week in Canada

**Joint Meeting
186th Meeting of the Acoustical Society of America
and the Canadian Acoustical Association**

Ottawa, Ontario, Canada
13-17 May 2024

***Noise: Paper 1pNSa1**

Flyback sonic booms from Falcon-9 rockets: Measured data and some considerations for future models

Mark C. Anderson, Kent L. Gee and Kaylee Nyborg

*Department of Physics and Astronomy, Brigham Young University, Provo, UT, 84602;
mark.anderson@byu.net; kentgee@byu.edu; kaylee.nyborg@byu.edu*

The SpaceX Falcon-9 rocket is a partially-reusable vehicle with a first-stage booster that lands propulsively after launch. As the booster falls toward the landing site, it produces a sonic boom. These sonic booms have unique properties and, so far, the ability to model them using current methods remains unclear. This paper presents findings from three Falcon-9 flyback sonic booms and highlights some features and trends that will be important to future modeling efforts. At every measurement location, a triple boom is recorded. This triple boom appears to propagate stably to at least 25 km from the landing pad. Within 1–2 km of the landing pad, the calculated sonic boom metrics tend to plateau. Outside 1–2 km of the launch and landing facility, the sonic boom is the highest-pressure event of the entire flight, including the launch. The Perceived Level 1 km from the landing pad is around 128 dB and at 25 km is around 87 dB. An appendix is included that discusses the benefits and challenges of attempting to correct for hardware low-frequency rolloff using digital pole-shift filtering.

***POMA Student Paper Competition Winner**



1. INTRODUCTION

To reduce costs and increase launch cadence, Space Exploration Technologies Corporation (SpaceX) flies the partially-reusable Falcon-9 rocket (SpaceX, 2024). The Falcon 9 has two stages: a booster that lifts the payload high into the atmosphere and a second stage that carries the payload to orbit. After the booster stage of flight is complete, the booster falls back through the atmosphere to land either on an ocean platform or back near the launch facility. Both the launch and landing phases of the flight are shown below in Fig. 1. In this paper, the term “launch” is reserved for the ascent portion, the term “flyback” refers to the booster’s descent through the atmosphere toward the landing location either on land or at sea, and the term “landing” indicates the brief powered descent right before the booster touches down. The term “flight” encompasses the launch, flyback, and landing.



Figure 1: (Left) A SpaceX Falcon-9 rocket shortly after liftoff. (Right) A Falcon-9 first-stage booster landing. Credit for both photos: SpaceX (CC BY-NC 2.0 DEED License. No changes made).

During the Falcon-9 booster flyback, the booster descends from heights over 100 km at supersonic speeds, producing a sonic boom that can be observed for at least 25 km around the landing location (FAA, 2020; Durrant *et al.*, 2023; Anderson and Gee, 2024). These sonic booms have three primary shocks (often referred to as a “triple boom”), rather than the two normally associated with far-field sonic booms (Maglieri *et al.*, 2014). Durrant *et al.* (2022) found that 8 km from the launch and landing facility at Vandenberg Space Force Base (VSFB), the A-weighted sound exposure level (ASEL) for the sonic boom over 650 ms was 99 dB while the ASEL for the 27 highest-amplitude seconds of launch noise was 100 dB. Thus, while the sonic boom is brief compared to the launch noise, the overall sound exposure between the two can be comparable in the far field. Durrant *et al.* (2023) analyzed that same sonic boom measured at distances from around 0.3–14 km from the launch and landing facility. They found that at the farthest measurement stations, the ASEL for the sonic boom tended to be comparable to the ASEL over the 6 dB-down period of the launch noise. Additionally, they discovered that at distances greater than about 1 km from the launch and landing facility, the sonic boom tended to become the highest-pressure event observed during the flight. Similar results were found by Anderson and Gee (2024), with the sonic boom being observed 25 km from the landing pad.

A Federal Aviation Administration (FAA) report from 2020 briefly discusses the sonic boom modeling approaches used by SpaceX (FAA, 2020). When using NASA’s PCBoom software in 2015 (Lonzaga *et al.*, 2022; Page *et al.*, 2023), SpaceX found that PCBoom tended to underestimate the near-field peak overpressures unless they used precise atmospheric information. SpaceX had more success using an adapted form of NASA’s 1122 simplified sonic boom prediction method (Carlson, 1978). This adapted method, named “SpaceX 1122” within the report, included “... expansion of the geometry and simplifying relations to estimate the wave propagation to the ground”. The SpaceX 1122 method tended to overestimate peak overpressures near the landing site but was deemed better overall. Their conclusion, as stated in the report, is

“SpaceX has measured and analyzed land landing overpressure data since 2015 and continues to rigorously optimize their adapted 1122 [model] to provide the most accurate and appropriate prediction for sonic boom data of a spacecraft vertical landing. [PCBoom] has been used in several instances and unless

calibrated to account for precise atmospheric factors, this model can underpredict peak overpressures for Falcon first stage boosters. SpaceX believes the adapted 1122 model represents the most applicable overpressure predictions based on the accuracy of the results discussed above and the previous approved use in environmental consultations. SpaceX believes the precision would remain the same for the future Falcon 9 first stage booster landings, with the highest peak overpressure remaining between 6-7 psf. Based on the precision of the data presented, similar re-entry trajectories with the same vehicle would result in similar sonic boom magnitudes.” (FAA, 2020)

Although the SpaceX 1122 model seems simpler than the PCBoom model and may work for Falcon-9 peak overpressures, it may not generalize to other vehicles. Because the model appears to be tailored to match measured Falcon-9 peak-overpressure data, other waveform parameters might not be as accurately predicted. For example, the NASA 1122 model uses “. . . the assumption that the pressure signal generated by the aircraft is of the far-field type, the classical N-wave.” (Carlson, 1978). Because the Falcon-9-booster flyback booms are not N-waves, any model based on NASA 1122 might not produce an accurate waveform shape. Predicting the triple boom may be particularly challenging because, to the authors’ knowledge, no prediction of a triple-boom waveform from a Falcon-9 booster currently exists in the public literature.

The purpose of this paper is to begin moving towards a more physical understanding of sonic booms produced by Falcon-9 rockets during flyback, in the hope that the global sonic boom community can begin to understand the physics behind these unique sonic booms. As more organizations fly and land reusable rockets, an understanding of the sonic booms produced will enable more-accurate predictions for effects on the community, wildlife, and structures. Additionally, future reusable rockets may incorporate more-precise predictions for sonic booms into the design process. To move toward these goals, this paper compiles three Falcon-9 sonic boom measurement campaigns performed at VSBF. These data can serve as a limited benchmark database for modeling Falcon-9 flyback sonic booms. The measurements are discussed in Section 2. The boom duration and shock positions are discussed in Section 3. Various sonic-boom metrics, including peak overpressures, rise times, and the National Aeronautics and Space Administration’s (NASA) human perception metrics (Loubeau and Page, 2018), are shown in Section 4. A brief comparison to the launch noise is shown in Section 5. Lastly, the Appendix includes a discussion on the benefits and challenges of using digital pole-shift filtering to correct for hardware low-frequency rolloff (Rasband *et al.*, 2023; Marston, 2008).

2. MEASUREMENTS

Brigham Young University (BYU) and California State University at Bakersfield (CSUB) completed three measurement campaigns to analyze the noise from different Falcon-9 flights at Vandenberg Space Force Base, CA. These measurements were performed during the SARah-1, Transporter-8, and SDA Tranche-0B missions. The SARah-1 and Transporter-8 measurements have been documented in greater detail by Durrant *et al.* (2023) and Anderson and Gee (2024) respectively, and the present paper builds on many of the similar analyses from those papers by including multiple measurement campaigns. The SDA Tranche-0B measurement used the same types of hardware and microphone configurations as the other measurements. Two representative field setups are shown in Fig. 2. The microphone is inverted and placed above a convex, circular, plastic ground plate. The microphone is protected from wind and rain by a domed windscreen. Other electronics are kept in a weather-robust case. These setups have been specifically designed for rocket launch and sonic boom measurements (James *et al.*, 2020; Gee *et al.*, 2020) and have been used in many launch vehicle noise data collection efforts (Hart *et al.*, 2022; Cunningham *et al.*, 2023; Gee *et al.*, 2023; Mathews *et al.*, 2023). As shown in Fig. 3, measurement stations, some of which were repeated across different flights to enable direct comparisons, were located between 0.3 and 25 km from the launch and landing facility. Because the peak frequency for these sonic booms is around 2–3 Hz (Anderson and Gee, 2024), digital pole-shift filtering was applied to all the measured data to improve the low-frequency responses (Rasband *et al.*, 2023; Marston, 2008). The Appendix contains further details on this process.

3. THE TRIPLE BOOM

A unique feature of Falcon-9 booster flyback sonic booms is their triple-boom shape. Figure 4 shows waveforms measured during the three flights at two consistent locations. Although the waveforms do not match perfectly between flights, they all have three main shocks. Perhaps these triple booms could also be referred to as “M-waves”, which would closely connect them to classical “N-waves” while still emphasizing their triple-boom shape.



Figure 2: Example measurement station consisting of an inverted microphone placed over a hard plastic ground plate and covered by a dome windscreen, with all other electronics placed inside a weather-resistant case. Some locations also included small weather stations mounted on tripods.

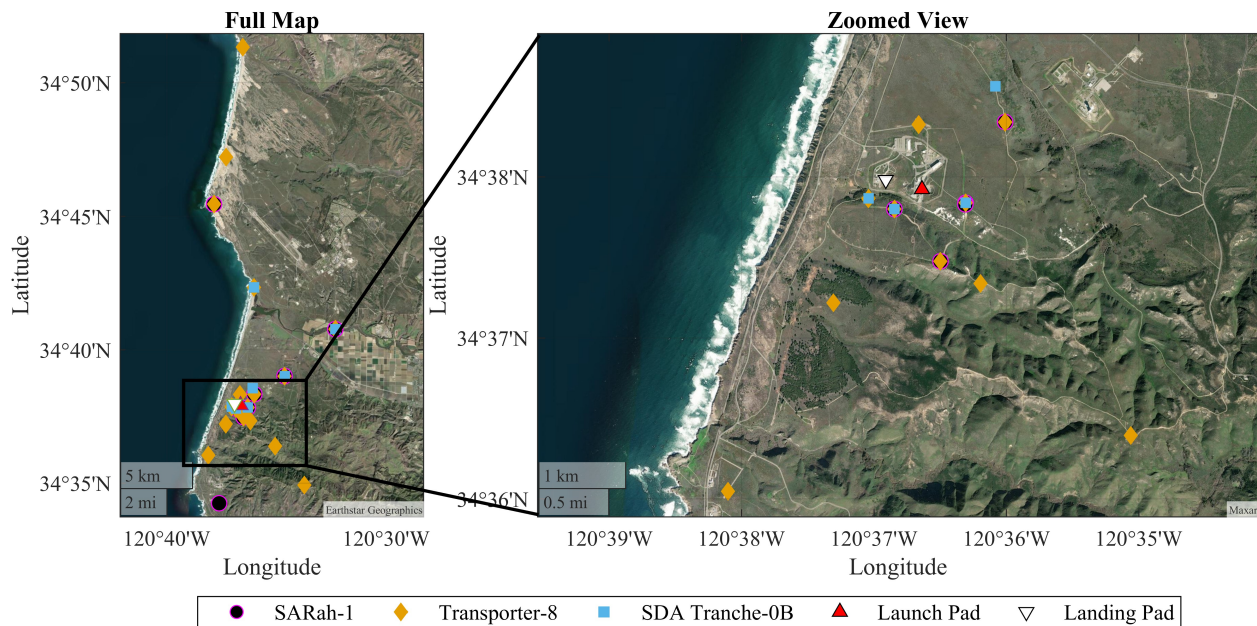


Figure 3: Measurement locations for the three flights. (Left) The full map. (Right) A zoomed-in map showing the stations nearest the pads. Imagery credit: Earthstar Geographics and Maxar.

The triple boom is measured at every location for the three flights. Although similar-looking waveforms can be produced when an aircraft is accelerating along a flight track (Page *et al.*, 2015), such booms are produced only at a few locations, ruling out the possibility that the Falcon-9 booster’s triple boom is the byproduct of sonic boom focusing due to acceleration. Another possible explanation was given by a SpaceX spokesperson, saying,

“[The] first boom is from the aft end (engines) . . . [The] second boom is from the landing legs at the widest point going up the side of the rocket. [The] third boom is from the fins near the forward end.” (Johnson, 2016)

This explanation deserves closer inspection, as it invites questions that may highlight future research needs. For reference, a schematic of the Falcon-9 booster during flyback is given in Fig. 5. The convex curvature near the widest point along a supersonic body tends to produce a rarefaction wave as discussed by Landau and Lifshitz (1987, Chap. 11) and Anderson (2017, Chap. 9), rather than a shock wave. This would indicate that the widest point of the folded

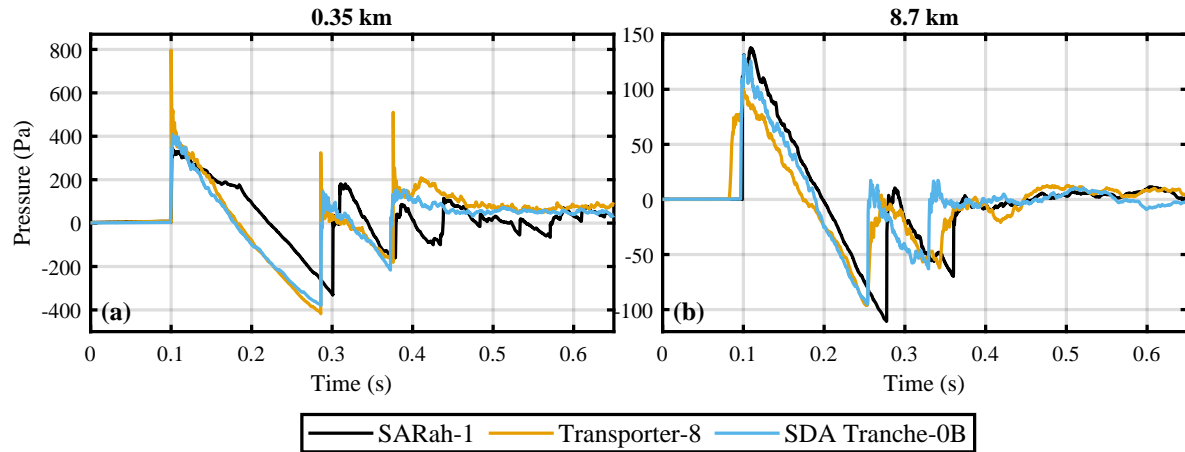


Figure 4: Example sonic boom waveforms from the three flights at distances of (a) 0.35 km and (b) 8.7 km from the landing pad. In (a) the SARah-1 third shock is partially conflated with noise produced by the booster engines, which are ignited shortly before the landing.

landing legs is an unlikely source for a strong shock. However, perhaps the intended meaning is that the shocks produced by various portions near the top and bottom of the folded landing legs do account for the center shock. There are computational fluid dynamics simulations and wind tunnel experiments that support this theory (Bykerk *et al.*, 2022; Marwege *et al.*, 2019). During propagation, these shocks may coalesce into a single shock and account for the middle shocks seen in Fig. 4. As for the grid fins, Durrant *et al.* (2022) argue that a small shock located shortly before the third shock could be caused by the grid fins while the final shock actually originates at the top of the interstage. This small shock is observed at several locations in the three measurements presented in this paper, but not all. While there can be many theories for the triple boom origin, no full simulations starting from vehicle geometry and including propagation have been published, making it difficult to understand at present exactly what causes the triple boom.

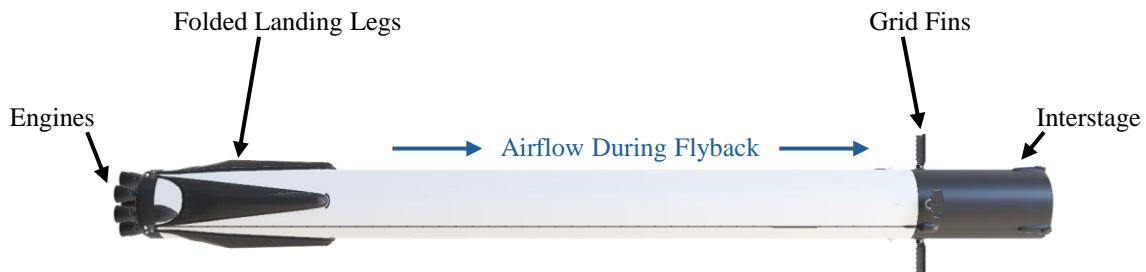


Figure 5: A schematic of the Falcon-9 booster during the flyback. The engines face the oncoming air. The landing legs remain folded until just before touchdown after the vehicle is subsonic. The grid fins are located near the bottom of the hollow interstage. 3D model adapted from Stanley Creative (2023) (CC BY 4.0 DEED License. Changes made).

The shock locations in the waveforms tend to be consistent at most measurement stations, as demonstrated in Fig. 6. Subplot (a) shows the total boom duration, or the time from the first shock to the third shock, while subplots (b) and (c) show the time between the first and second shocks, then the second and third shocks respectively. Most of the variability occurs between the first and second shocks, while the second and third shocks appear to generally have a constant time difference. The fact that booms measured 0.3 km and 25 km from the landing pad have nearly same duration is surprising because sonic booms tend to elongate with propagation distance (Maglieri *et al.*, 2014). While the sonic booms do not originate at the pad, but rather at some higher altitude, the sonic boom likely travels substantially farther to the farthest measurement stations than to the stations closer to the landing site. It is possible that waveform freezing may help account for the consistent shock locations (McLean, 1965; Hayes, 1967; Hayes *et al.*, 1968; Cleveland and Blackstock, 1996).

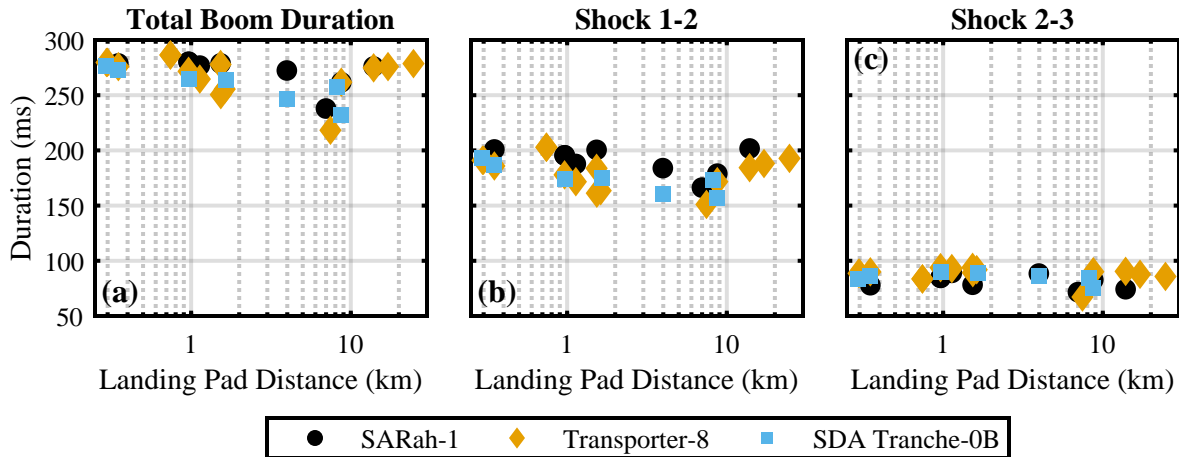


Figure 6: Duration between shocks. (a) The time between first and third shocks, or the total boom duration. (b) Time between first and second shocks. (c) Time between the second and third shocks.

4. METRICS

A. PEAK PRESSURE AND RISE TIME

Analyzing the peak overpressure data from these three flights enables a direct comparison with measured SpaceX data (FAA, 2020). This comparison is shown in Fig. 7. Farther than about 8 km from the landing pad, the sonic boom peak overpressures from these flights agree with the SpaceX measured data. Closer to the landing pad, all sonic boom peak overpressures from these three launches are consistently higher than the SpaceX data. The reason for this difference is unknown, but could be due to different return trajectories at VSFb compared to the Florida launch and landing sites, where the SpaceX data were obtained. It is also possible that the Falcon-9 booster design or typical landing trajectory has evolved enough to account for the difference since the time when these data were taken by SpaceX. Also noteworthy is the outlier at about 16 pounds per square foot (psf), the waveform for which is shown in Fig. 4(a) above. This particular waveform seems to have undergone turbulence-induced focusing, something common for other sonic booms (Maglieri and Sothcott, 1990; Maglieri *et al.*, 2014; Stout *et al.*, 2021). Other waveforms from these measurements show similar, less dramatic, signs of distortion. A study of how atmospheric turbulence affects Falcon-9 sonic booms has only recently begun (Nyborg *et al.*, 2024).

The rise times for these sonic booms are difficult to define. Typically, a sonic boom rise time is calculated by using the time between 10% – 90% of the peak overpressure (Maglieri *et al.*, 2011). As illustrated in Fig. 8(a), this definition has problems when the shock does not reach 90% of the waveform peak overpressure. This is a common occurrence for the Falcon-9 sonic booms measured during these three flights, where the true peak overpressure arrives after a delay that can be around one to two orders of magnitude longer than the rise time of the shock. To work around this problem, Fig. 8(b) shows the front shock rise time from 10% – 50% of the waveform peak overpressure, denoted as the “half-rise time”. It is unlikely that this is the optimal approach to calculating the rise time, but it is sufficient for the present analysis to begin observing trends.

For both the peak overpressures and front shock rise times, the data tend to plateau within about 1–2 km from the landing pad. This is also true for the metrics shown later in this paper. A similar trend was noted by Durrant *et al.* (2023), but because only the SARah-1 data were considered for that paper, the sparsity of data resulted in the potentially-flawed conclusion that the sonic boom had a slower, cylindrical geometric decay rate. While sonic booms are generally considered to be cylindrical waves (Maglieri *et al.*, 2014), the explanation by Durrant *et al.* (2023) used the launch pad as the distance reference point. Because the sonic booms do not originate on the ground, but at some higher altitude, the exact distance from the source is difficult to determine, complicating an accurate estimation of the decay rate with distance. Thus the slower decay rate observed by Durrant *et al.* (2023) is probably the byproduct of trying to fit the plateauing data, something difficult to foresee without additional measurements. Perhaps the raytracing in PCBoom can be used in the future to better estimate the distance from the source to the receiver. Then a more-complete analysis of decay rate with distance can be performed.

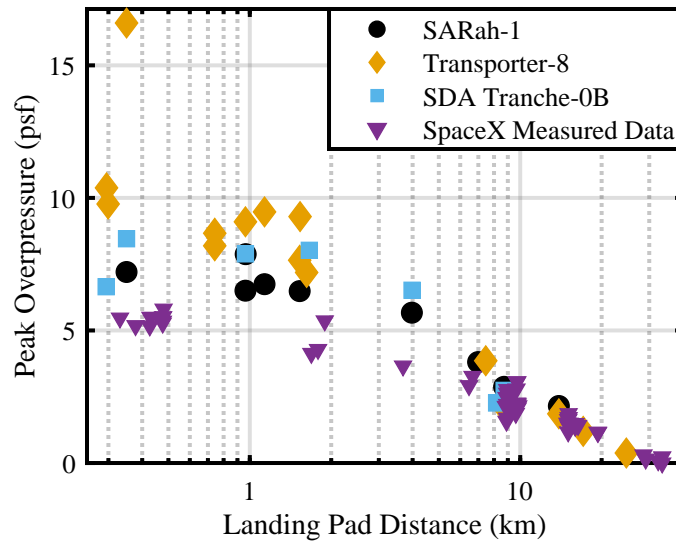


Figure 7: The sonic-boom peak overpressure in pounds per square foot as a function of distance from the landing pad. The SpaceX data are digitized from FAA (2020).

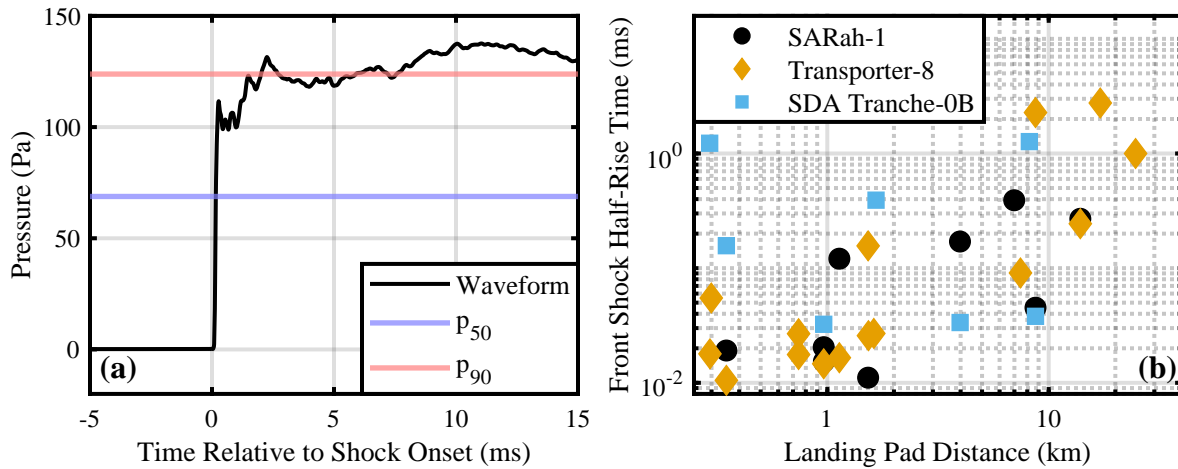


Figure 8: (a) An example waveform from SARah-1 at 8.7 km from the landing pad, illustrating that the p_{90} , or the point where the waveform reaches 90% of its peak overpressure, occurs after the first shock. The point where 50% of the peak pressure (p_{50}) is obtained is used in part (b) where sonic-boom front shock half-rise time for the three flights are shown as a function of distance from the landing pad.

Although not as rigorous as ray-tracing software, the plateau in the data can be qualitatively explained by considering the vehicle trajectory (Anderson and Gee, 2024). When viewing the live telemetry data (SpaceX, 2023), the booster tends to become subsonic while still a few kilometers above the landing site. Therefore, the rays intersecting the ground near the landing pad must be generated at these altitudes. Because all the locations near the pad are roughly equidistant from the source, the sonic booms that reach those locations will all have propagated a similar distance, which could produce sonic booms with similar properties. For the farther measurement stations, the rays are generated higher and have more horizontal range to cover before reaching these locations, which could account for an overall decay in metric values with increased distance from the landing pad. This explanation qualitatively accounts for the plateau in metric values near the landing pad and the decay in metric values at farther distances.

B. NASA SONIC BOOM HUMAN PERCEPTION METRICS

NASA has determined several sonic boom metrics that tend to correlate with human annoyance (Loubeau and Page, 2018). These are the A-, B-, D-, and E-weighted sound exposure levels (SEL), a modified version of the Steven's Mark VII perceived level of loudness (PL) (Stevens, 1972; Shepherd and Sullivan, 1991), and the Indoor Sonic Boom Annoyance Predictor (ISBAP). The weighted SEL metrics, and including the C- and Z-weightings for completeness, are shown in Fig. 9. These metrics all tend to plateau at closer distances to the launch pad, as discussed above for the peak overpressure and rise time. Because these metrics are frequently calculated, providing them in this paper enables comparisons to other sonic booms.

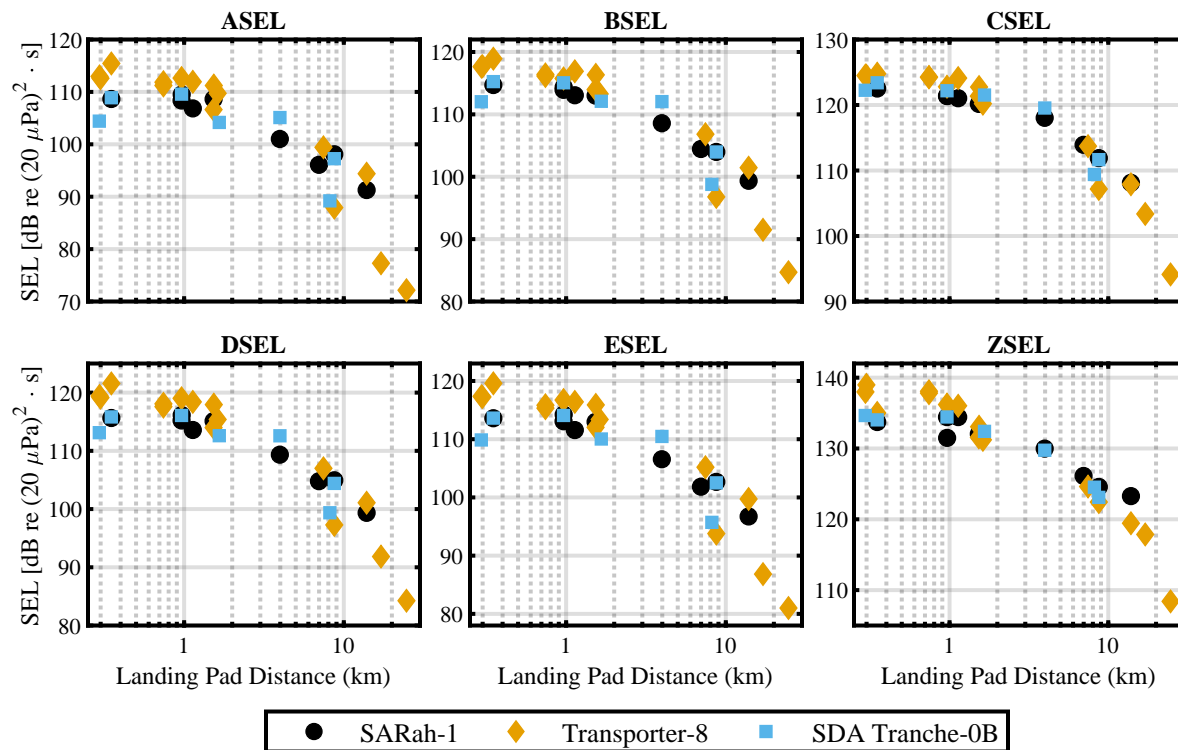


Figure 9: Six different sound exposure level weightings for the sonic booms from the three flights. The subplot titles denote which weighting is shown in each plot.

NASA's sonic boom metrics include two non-SEL measures, PL and ISBAP, which are both shown in Fig. 10. Included in Fig. 10(a) is the NASA target value for the X-59 quiet supersonic demonstrator (Doebler and Rathsam, 2020; NASA, 2023), indicating that the Falcon-9 sonic boom PL values are still about 10 dB higher than the target X-59 value at distances up to 25 km from the landing pad. Doebler and Rathsam (2020) performed several experiments to help readers mentally calibrate the PL metric with other experiences. For example, a PL of 115 dB, about the same as being 5–10 km from the landing pad, is equivalent to a firework exploding 500 ft away. Personal experience by the authors indicates that this comparison would be accurate for fairly large fireworks. Doebler and Rathsam (2020) also state that a PL of 125–130 dB, which occurs within about 2 km from the landing pad, is approximately equivalent to a gunshot measured from 2 ft away (without hearing protection). The authors have not come across X-59 targets for the other NASA sonic boom metrics.

Although these metrics are commonplace in aircraft sonic boom analyses because of their correlations with human perception, the authors know of no subjective studies of human or animal response to these unique Falcon-9 triple booms. Additionally, the NASA-modified PL metric carries with it the assumption of only two shocks (Shepherd and Sullivan, 1991), so its suitability for sonic booms with three shocks is unclear. This same problem arises for the ISBAP, which uses the PL as an input (Loubeau and Page, 2018).

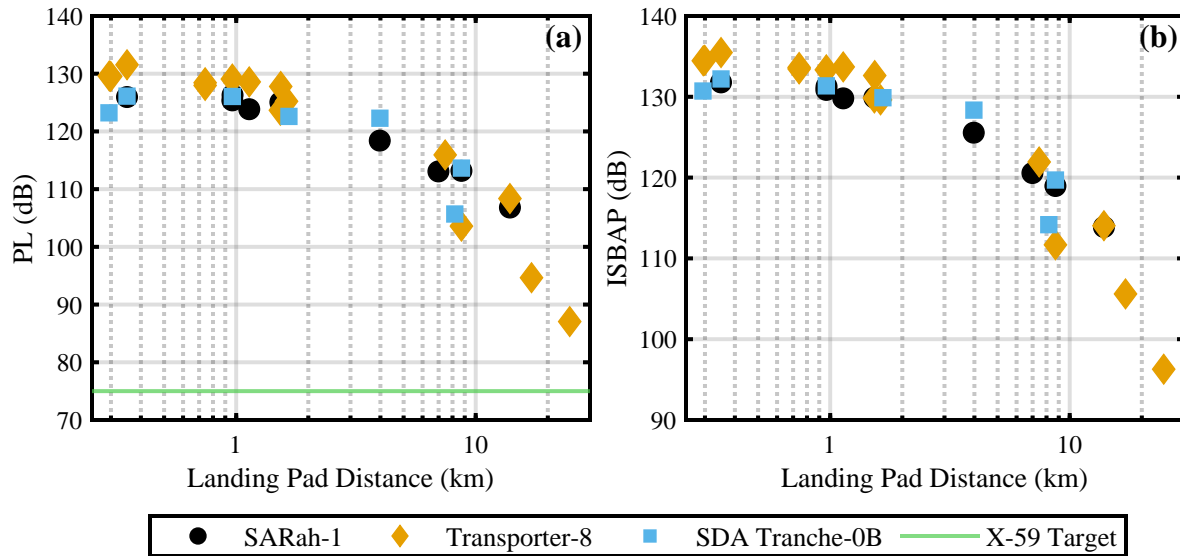


Figure 10: The (a) Perceived Level (PL) and (b) Indoor Sonic Boom Annoyance Predictor (ISBAP) for the sonic booms from the three flights. Also included in (a) is the target PL for NASA’s X-59 quiet supersonic demonstrator aircraft (Doebler and Rathsam, 2020; NASA, 2023).

5. COMPARISON TO LAUNCH NOISE

The sonic boom represents a noise source comparable to the launch. Figure 11(a) shows the peak pressures for the launch and the sonic boom as a function of distance. Farther than 1–2 km, the sonic boom is the highest-pressure event of the entire flight, and that trend persists to at least 25 km. Figure 11(b) shows the ZSEL values calculated over the entire launch and the sonic boom. Farther than about 5 km, the sonic boom ZSEL can be comparable to the launch ZSEL. In other words, at those distances, the short 650-ms sonic boom recording can deliver as much sound exposure as the entire launch that precedes it. The ASEL is calculated the same way and is shown in Fig. 11(c). Farther than about 8 km, the sonic boom ASEL can be comparable to the launch ASEL, but not in every case. However, it is worth noting that the ASEL is unlikely to truly capture the human perception of either the launch or the sonic boom, considering that it essentially neglects the low peak frequencies for both (Gee *et al.*, 2023).

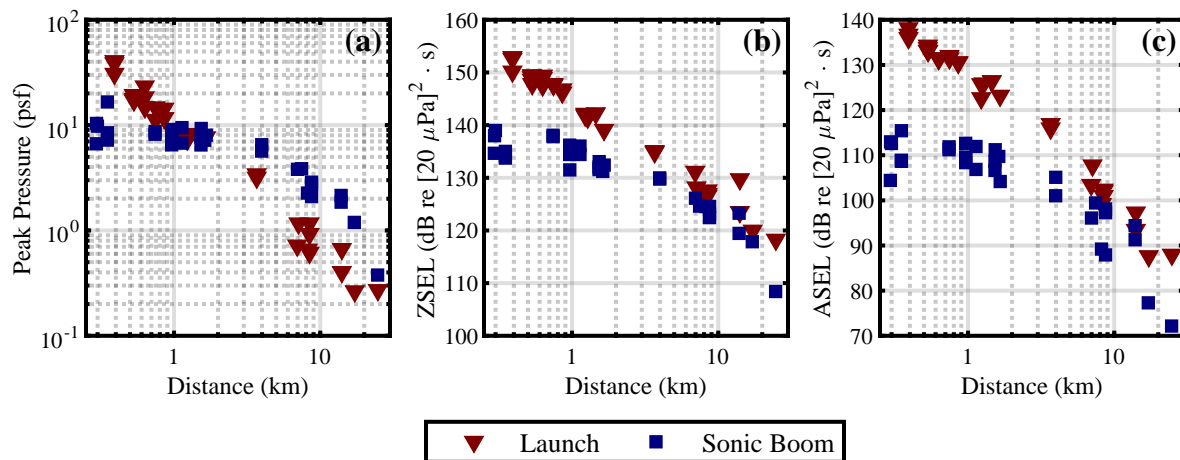


Figure 11: Comparing the (a) peak pressure, (b) ZSEL, and (c) ASEL between the launches and sonic booms. All three datasets have been combined for simplicity in these plots. The launch distance is relative to the launch pad and the sonic boom distance is relative to the landing pad.

6. CONCLUSION

The sonic booms produced by Falcon-9 boosters during flyback are unique compared to traditional aircraft sonic booms. At every measurement location for three different flights a triple-boom shape is observed. This unique triple boom appears to propagate stably with minimal shock movement or coalescence within the waveform out to at least 25 km from the landing site. All sonic boom metrics tend to plateau within 1–2 km of the landing site, and only decrease with distance for observers outside this radius.

When considering the peak pressure amplitudes and total sound exposure during a flight, the flyback sonic boom should be considered a major contribution. Farther than 1–2 km from the launch and landing facility, which are nearly collocated at VAFB, the sonic boom peak overpressure exceeds the peak pressures observed during the launch. Farther than 5 km from the facility, the ZSEL for the sonic boom alone can be comparable to the ZSEL over the entire launch preceding the sonic boom. Additionally, the sonic boom perceived level can exceed NASA's current criterion estimate for human annoyance at distances as far as 25 km from the landing site.

Much work remains to be done in the area of launch vehicle flyback sonic booms. Both NASA's PCBoom software and SpaceX's modified NASA 1122 method have struggled to accurately predict the peak overpressures near the landing site (FAA, 2020). Perhaps this is related to the metric plateau observed near the landing pad. Additionally, the ability to model a triple sonic boom from a booster flyback has not yet been clearly demonstrated within the scientific literature. So far, Falcon-9 sonic boom predictions and validations appear to have focused primarily on peak overpressures. While this is a good start, sonic boom perception is influenced by more than the peak overpressure alone, depending strongly on the shock rise times that determine the high-frequency energy content (Loubeau and Page, 2018).

A thorough understanding of the sonic booms produced during flyback will be essential as other organizations design and fly reusable launch vehicles. The ability to predict not just the peak overpressure, but also the full waveform and spectrum, will enable more-accurate environmental assessments. It may also become possible to intentionally alter the sonic boom shapes during the vehicle design process to better accommodate the local environmental and community noise criteria. As reusable rockets fly more frequently, research into the flyback sonic booms will enable a more-reliable approach to understanding the effects on structures, wildlife, and communities.

ACKNOWLEDGMENTS

The measurements for this work were funded by the US Air Force/Space Force and supported by USACE. We gratefully acknowledge tireless logistical and other support from members of SLD-30.

The analyses for this work were funded by an appointment to the Department of Defense (DOD) Research Participation Program administered by the Oak Ridge Institute for Science and Education (ORISE) through an interagency agreement between the U.S. Department of Energy (DOE) and the DOD. ORISE is managed by ORAU under DOE contract number DE-SC0014664. All opinions expressed in this paper are the author's and do not necessarily reflect the policies and views of DOD, DOE, or ORAU/ORISE.

APPENDIX: EXTENDING MEASUREMENT BANDWIDTH TO LOWER FREQUENCIES

Because the sound levels are highest near the launch and landing facility, quarter-inch microphones were used at closer locations. However, these microphones roll off at higher frequencies than the half-inch microphones used at farther stations. Failing to accurately measure the low frequencies results in a distorted waveform. By assuming a low-frequency rolloff shape, the waveform and spectrum can be approximately restored using digital pole-shift filtering (Rasband *et al.*, 2023; Marston, 2008). A distorted waveform example from the Transporter-8 measurement is shown in Fig. 12, where two different microphones were deployed at the same location. One of the channels used a GRAS 47AC with a manufacturer-specified low-frequency cutoff of 0.09 Hz (GRAS, 2024b) and the other channel used a GRAS 46BE with a manufacturer-specified low-frequency cutoff of about 4 Hz (GRAS, 2024a). The GRAS 47AC channel, indicated in black in Fig. 12, most accurately resolves the true waveform shape. The GRAS 46BE channel, indicated in pink, has curved ramps between the shocks and tends to overshoot the peak pressures on the second and third shocks. After applying digital pole-shift filtering, the GRAS 46BE channel better approximates the GRAS 47AC measurement. This result is shown in green. Throughout this paper, digital pole-shift filtering has been applied to all the data to approximately account for the low-frequency rolloff of both the microphones and data acquisition systems. In the future, the microphone responses can be precisely measured and a more-accurate correction can be applied.

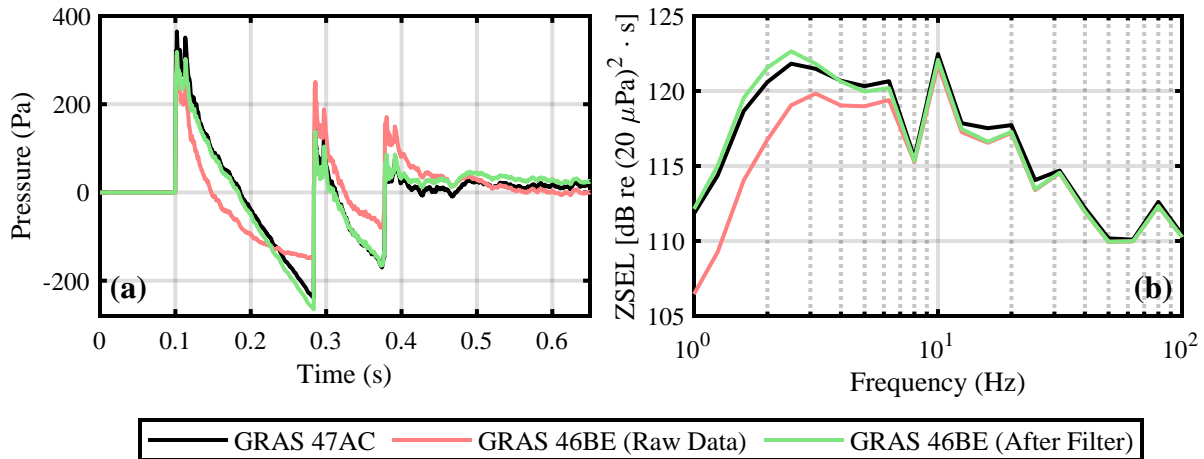


Figure 12: An example of restoring the low-frequency content in a sonic boom measurement. The colors represent channels using a GRAS 47AC (black), GRAS 46BE (pink), and the same GRAS 46AE after applying digital pole-shift filtering (green). Both channels used an NI 9250 card. (a) The waveforms. (b) The low-frequency spectra.

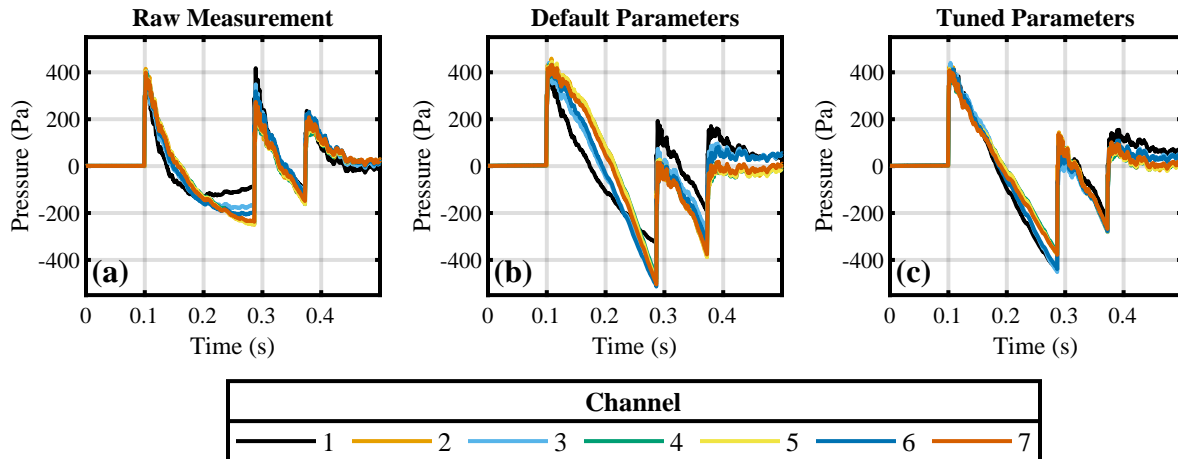


Figure 13: The effects of digital pole-shift filtering with different input parameters. (a) No filter applied. (b) The manufacturer-specified cutoff frequencies are used. (c) The cutoff frequencies have been tuned so the ramps between the first and second shocks are approximately linear.

Digital pole-shift filtering with quarter-inch microphones is challenging. Experience working with these microphones has indicated that the optimal cutoff frequency to use in the filter can deviate somewhat from the manufacturer specifications. This was noted by Rasband *et al.* (2023) to a lesser degree for half-inch microphones. For example, the published cutoff frequency for the GRAS 46BE microphone is 4 Hz (GRAS, 2024a), but in Fig. 12, an assumed input cutoff of 2.6 Hz was used to produce the green curves because it produced a closer match to the GRAS 47AC channel. To study this further, Fig. 13 shows sonic boom measurements using a seven-microphone probe deployed near the launch and landing facility during the SDA Tranche-0B measurement. These channels used GRAS 46BD microphones on NI 9250 cards. Figure 13(a) shows the raw measured data, with no attempt to correct the low-frequency response. Figure 13(b) shows the waveforms after digital pole-shift filtering with the default parameters as inputs (0.43 Hz for the NI 9250 card and 4.0 Hz for the GRAS 46BD). The low-frequency responses of the card and microphone were brought down using digital pole-shift filtering to 0.13 Hz and 0.10 Hz respectively. The waveforms are still somewhat distorted and don't agree with each other. Figure 13(c) shows the results after the input cutoff frequencies for the microphones have been tuned to produce a roughly-linear expansion between the first two shocks. These tuned parameters produce closer agreement between channels. The tuned cutoff frequencies, along with the peak overpressures,

21 November 2024 19:12:24

ZSEL, and ASEL for each channel in each subplot are shown in Table 1. The peak overpressure and ZSEL show the greatest sensitivity to the inputs, while the ASEL is hardly affected. This is because digital pole-shift filtering only affects the lowest frequencies, so metrics that tend to omit the low frequencies are not strongly impacted. The mean and standard deviations are also given in Table 1, providing an estimate of the uncertainty in each case. To simplify the analyses, the manufacturer specifications for cutoff frequency have been used throughout this paper rather than custom-tailoring each channel. The uncertainties are not large enough to negate the trends observed in this paper.

Table 1: Metrics corresponding to all the waveforms in Fig. 13. Although those are plots trimmed in time, the metrics were calculated over the full 650-ms windows. The mean and standard deviation for each column is shown.

Channel	Tuned Cutoff (Hz)	Peak Overpressure (Pa)			ZSEL (dB)			ASEL (dB)		
		Raw	Default	Tuned	Raw	Default	Tuned	Raw	Default	Tuned
1	6.0	417.5	405.1	415.9	131.7	134.0	135.8	108.9	108.9	108.9
2	2.0	414.9	458.4	423.4	133.2	136.6	134.3	108.6	108.6	108.6
3	4.0	404.7	440.1	440.1	132.6	135.6	135.6	108.9	108.9	108.9
4	2.0	392.5	431.8	412.1	132.9	136.4	134.1	108.4	108.5	108.4
5	2.0	404.4	444.6	413.8	133.2	136.6	134.3	108.9	108.9	108.9
6	3.0	387.4	432.1	412.5	133.2	136.5	135.4	108.7	108.8	108.7
7	2.0	399.5	431.8	408.7	133.1	136.5	134.3	108.6	108.6	108.6
Mean	3.0	403.0	434.8	418.1	132.8	136.0	134.8	108.7	108.7	108.7
Stdev	1.5	11.0	16.3	10.7	0.6	1.0	0.7	0.2	0.2	0.2

REFERENCES

- Anderson, J. D. (2017). McGraw-Hill Series in Aeronautical and Aerospace Engineering *Fundamentals of Aerodynamics*, 6th ed. (McGraw-Hill Education).
- Anderson, M. C., and Gee, K. L. (2024). "Sonic Boom Measurements From the SpaceX Transporter-8 Falcon-9 Rocket Landing at Vandenberg Space Force Base," in *30th AIAA/CEAS Aeroacoustics Conference*, AIAA, <https://doi.org/10.2514/6.2024-3188>. Corrections to a few errors in the manuscript can be found at <https://doi.org/10.2514/6.2024-3188.c1>.
- Bykerk, T., Kirchheck, D., and Karl, S. (2022). "Reconstruction of Wind Tunnel Tests using CFD for a Reusable First Stage during Rocket Retro-Propulsion," in *9th European Conference for Aeronautics and Space Sciences (EUCASS)*, <https://doi.org/10.13009/EUCASS2022-4494>
- Carlson, H. W. (1978). "Simplified Sonic Boom Prediction," Report, NASA-TP-1122.
- Cleveland, R. O., and Blackstock, D. T. (1996). "Waveform Freezing of Sonic Booms Revisited," in *1995 NASA High-Speed Research Program Sonic Boom Workshop*, edited by D. G. Baize, Vol. 1, pp. 20–40.
- Cunningham, C., Anderson, M. C., Moats, L. T., Gee, K. L., Hart, G. W., and Hall, L. K. (2023). "Acoustical measurement and analysis of an Atlas V launch," in *182nd Meeting of the Acoustical Society of America*, Proc. Mtgs. Acoust., Vol. 46, <https://doi.org/10.1121/2.0001742>
- Doebler, W. J., and Rathsam, J. (2020). "How loud is X-59's shaped sonic boom?," Proc. Mtgs. Acoust., Vol. 36, <https://doi.org/10.1121/2.0001265>
- Durrant, J. T., Anderson, M. C., Bassett, M. S., Gee, K. L., Hart, G. W., Batelaan, R. H., Lawrence, D. C., and Hall, L. K. (2023). "Overview and spectral analysis of the Falcon-9 SARah-1 launch and reentry sonic boom," in *184th Meeting of the Acoustical Society of America*, Proc. Mtgs. Acoust., Vol. 51, <https://doi.org/10.1121/2.0001767>
- Durrant, J. T., Anderson, M. C., Gee, K. L., Mathews, L. T., and Hart, G. W. (2022). "Initial comparison of a Falcon-9 reentry sonic boom with other launch-related noise," in *182nd Meeting of the Acoustical Society of America*, Proc. Mtgs. Acoust., Vol. 46, <https://doi.org/10.1121/2.0001579>
- FAA (2020). "Final Environmental Assessment and Finding of No Significant Impact for SpaceX Falcon Launches at Kennedy Space Center and Cape Canaveral Air Force Station, Appendix A," Report, www.faa.gov/sites/faa.gov/files/space/environmental/nepa_docs/Falcon_Program_EA_Appendices_508.pdf.
- Gee, K. L., Hart, G. W., Cunningham, C. F., Anderson, M. C., Bassett, M. S., Mathews, L. T., Durrant, J. T., Moats, L. T., Coyle, W. L., Kellison, M. S., and Kuffskie, M. J. (2023). "Space Launch System acoustics: Far-field noise measurements of the Artemis-I launch," *JASA Express Lett* 3(2), 023601, <https://doi.org/10.1121/10.0016878>

- Gee, K. L., Novakovich, D. J., Mathews, L. T., Anderson, M. C., and Rasband, R. D. (2020). "Development of a Weather-Robust Ground-Based System for Sonic Boom Measurements," Report NASA/CR-2020-5001870.
- GRAS (2024a). "GRAS 46BE 1/4" CCP Free-field Standard Microphone Set" www.grasacoustics.com/products/measurement-microphone-sets/constant-current-power-ccp/product/143-46be.
- GRAS (2024b). "GRAS 47AC 1/2" CCP Infra-Sound Microphone Set" www.grasacoustics.com/products/special-microphone/infra-sound-microphones/product/712-47ac.
- Hart, G. W., Mathews, L. T., Anderson, M. C., Durrant, J. T., Bassett, M. S., Olaussen, S. A., Houston, G., and Gee, K. L. (2022). "Methods and results of acoustical measurements made of a Delta IV Heavy launch," in *181st Meeting of the Acoustical Society of America*, Proc. Mtgs. Acoust., Vol. 45, <https://doi.org/10.1121/2.0001580>
- Hayes, W. D. (1967). "Brief Review of the Basic Theory," in *Sonic Boom Research*, edited by A. R. Seebass, NASA, pp. 3–7, NASA-SP-147.
- Hayes, W. D., Haefeli, R. C., and Kulsrud, H. E. (1968). "Sonic Boom Propagation in a Stratified Atmosphere with Computer Program," NASA-CR-1299.
- James, M. M., Salton, A., Calton, M., Downing, J. M., Gee, K. L., and McInerney, S. A. (2020). "Commercial Space Operations Noise and Sonic Boom Measurements," Report, <https://doi.org/10.17226/25834>
- Johnson, S. (2016). "From Double to Triple: Why the Landing Falcon 9 Creates Three Sonic Booms" www.spaceflightinsider.com/organizations/space-exploration-technologies/double-triple-landing-falcon-9-creates-three-sonic-booms/, This is the original source for the quote. The website is not available for reasons unknown to the authors at the time of this publication.
- Landau, L. D., and Lifshitz, E. M. (1987). *Fluid Mechanics*, 6 of *Course of Theoretical Physics* (Elsevier).
- Lonzaga, J. B., Page, J. A., Downs, R. S., Kaye, S. R., Shumway, M. J., Loubeau, A., and Doebler, W. J. (2022). "PCBoom 7 Technical Reference," Report, NASA/TM-20220007177.
- Loubeau, A., and Page, J. (2018). "Human Perception of Sonic Boom from Supersonic Aircraft," *Acoustics Today* 14(3), 23–30.
- Maglieri, D. J., Bobbitt, P. J., Plotkin, K. J., Shepherd, K. P., Coen, P. G., and Richwine, D. M. (2014). "Sonic Boom: Six Decades of Research," Report, NASA-SP-2014-622.
- Maglieri, D. J., Henderson, H. R., Massey, S. J., and Stansbery, E. G. (2011). "A Compilation of Space Shuttle Sonic Boom Measurements," Report, NASA/CR-2011-217080.
- Maglieri, D. J., and Sothcott, V. E. (1990). "Summary of Sonic Boom Rise Times Observed during FAA Community Response Studies over a 6-Month Period in the Oklahoma City Area," Report, NASA-CR-4277.
- Marston, T. M. (2008). "Diffraction Correction and Low-frequency Response Extension for Condenser Microphones," Thesis, The Pennsylvania State University.
- Marwege, A., Riemer, J., Klevanski, J., Gülhan, A., Ecker, T., Reimann, B., and Dumont, E. (2019). "First Wind Tunnel Data of CALLISTO - Reusable VTVL Launcher First Stage Demonstrator," in *EUCASS 2019*, <https://doi.org/10.13009/EUCASS2019-350>
- Mathews, L. T., Anderson, M. C., Gardner, C. D., McLaughlin, B. W., Hinds, B. M., McCullah-Boozer, M. R., Hall, L. K., and Gee, K. L. (2023). "An overview of acoustical measurements made of the Atlas V JPSS-2 rocket launch," in *184th Meeting of the Acoustical Society of America*, Proc. Mtgs. Acoust., Vol. 51, <https://doi.org/10.1121/2.0001768>
- McLean, F. E. (1965). "Some Nonasymptotic Effects on the Sonic Boom of Large Airplanes," Report, NASA-TN-D-2877.
- NASA (2023). "NASA Quesst Home" www.nasa.gov/mission/quesst/.
- Nyborg, K., Anderson, M. C., and Gee, K. L. (2024). "Turbulence-induced variability of a far-field Falcon-9 sonic boom measurement" Meeting Abstract, 186th Meeting of the Acoustical Society of America.
- Page, J., Plotkin, K. J., Hobbs, C., Sparrow, V., Salamone, J., Cowart, R., Salamone, J., Elmer, K., Welge, H. R., Ladd, J., Maglieri, D., and Piacsek, A. (2015). "Superboom Caustic Analysis and Measurement Program (SCAMP) Final Report," Report NASA/CR—2015–218871.
- Page, J. A., Lonzaga, J. B., Shumway, M. J., Son, S. R., Downs, R. S., Loubeau, A., and Doebler, W. J. (2023). "PCBoom 7.3 User's Guide," Report NASA/TM–20220016207.
- Rasband, R. D., Gee, K. L., Gabrielson, T. B., and Loubeau, A. (2023). "Improving low-frequency response of sonic boom measurements through digital filtering," *JASA Express Lett.* 3, <https://doi.org/10.1121/10.0016751>
- Shepherd, K. P., and Sullivan, B. M. (1991). "A Loudness Calculation Procedure Applied to Shaped Sonic Booms," Report, NASA-TM-107708.
- SpaceX (2023). "Transporter-8 Mission" www.youtube.com/watch?v=z03luySkHQ&t=853s.
- SpaceX (2024). "Falcon 9: First Orbital Class Rocket Capable of Reflight" www.spacex.com/vehicles/falcon-9/.
- Stanley Creative (2023). "Falcon 9 - SpaceX" sketchfab.com/3d-models/falcon-9-spacex-394f7cf52d124bbd9db69f24d1ff2f08.
- Stevens, S. S. (1972). "Perceived Level of Noise by Mark VII and Decibels (E)," *J. Acoust. Soc. Am.* 51(2B), 575–601, <https://doi.org/10.1121/1.1912880>
- Stout, T. A., Sparrow, V. W., and Blanc-Benon, P. (2021). "Evaluation of numerical predictions of sonic boom level variability due to atmospheric turbulence," *J. Acoust. Soc. Am.* 149(5), 3250, <https://doi.org/10.1121/10.0004985>